# Profile Controlled Gold Nanostructures Fabricated by Nanosphere Lithography for Localized Surface Plasmon Resonance

Xiaodong Zhou and Nan Zhang

***Abstract*—**Localized surface plasmon resonance (LSPR) is the coherent oscillation of conductive electrons confined in noble metallic nanoparticles excited by electromagnetic radiation, and nanosphere lithography (NSL) is one of the cost-effective methods to fabricate metal nanostructures for LSPR. NSL can be categorized into two major groups: dispersed NSL and closely pack NSL. In recent years, gold nanocrescents and gold nanoholes with vertical sidewalls fabricated by dispersed NSL, and silver nanotriangles and gold nanocaps on silica nanospheres fabricated by closely pack NSL, have been reported for LSPR biosensing. This paper introduces several novel gold nanostructures fabricated by NSL in LSPR applications, including 3D nanostructures obtained by evaporating gold obliquely on dispersed nanospheres, nanoholes with slant sidewalls, and patchy nanoparticles on closely packed nanospheres, all of which render satisfactory sensitivity for LSPR sensing. Since the LSPR spectrum is very sensitive to the shape of the metal nanostructures, formulas are derived and software is developed for calculating the profiles of the obtainable metal nanostructures by NSL, for different nanosphere masks with different fabrication conditions. The simulated profiles coincide well with the profiles of the fabricated gold nanostructures observed under scanning electron microscope (SEM) and atomic force microscope (AFM), which proves that the software is a useful tool for the process design of different LSPR nanostructures.

***Keywords*—**Nanosphere lithography, localized surface plasmon resonance, biosensor, simulation.

## I. INTRODUCTION

IN recent two decades, localized surface plasmon resonance (LSPR), a coherent oscillation of conductive electrons in nanostructured noble metal with light excitation, is broadly used for reflective index variation based biosensors [1]–[7], surface-enhanced spectroscopic methods such as surface-enhanced Raman spectroscopy (SERS) [8], [9], and killing of cancerous cells through plasmonic heating [10], [11].

In general, LSPR exists for all kinds of metal nanostructures. In LSPR, each metal nanostructure acts as an individual emitting element, and the oscillation peaks of the LSPR spectrum are determined by the shape, size,

interdistance, material of the nanostructures, as well as the adjacent media. Although single metal nanoparticle LSPR has been heavily investigated and demonstrated with the detection of biological samples, a large amount of nanostructures with identical shape and even distribution on an area with > 10 μm critical length are desired for practical applications, which potentiate the development of a LSPR chip into a microfluidic device or a microfluidic sensing array. Moreover, the fabrication of the nanostructures is also expected to be cost-effective, able to generate sharp corners on the nanostructures to enhance the plasmonic signal, and able to be fine tuned to control the oscillation peaks of the metal nanostructures.

Nanosphere lithography (NSL), which uses a group of dispersed or closely packed nanospheres on a substrate as a mask for nanostructure fabrication, is an ideal candidate for obtaining various nanoparticles or nanoholes for LSPR biosensing [12]–[32]. In reality, nanospheres are difficult to be dispersed or closely packed on a substrate; they tend to aggregate due to the strong capillary force among them. However, recent studies have facilitated the dispersion or close-pack of the nanospheres on various kinds of substrates. In dispersed NSL [12]–[20], the nanospheres are dispersed on a substrate, and each nanosphere serves as a separate mask for metal evaporation or metal etching; whereas in closely packed NSL [21]–[32], the nanospheres are closely packed in mono or multiple layers, the shadows of several adjacent nanospheres contribute to the formation of a nanostructure. NSL includes critical processes of nanosphere arrangement and metal evaporation, and optional subsequent processes of metal etching and nanosphere removal. Most importantly, any parameter in these processes will severely affect the shape of the nanostructures, thus the process control in NSL for obtaining the desired nanostructures becomes crucial.

In this paper, three novel metal nanostructures created in our group, including 3D nanostructures on dispersed nanospheres, nanoholes with slant sidewalls, and patchy nanoparticles on closely packed nanospheres, are reported for LSPR applications. A simulation method is introduced to correlate the profile of the nanostructures to the process conditions and parameters in NSL fabrication. The programmed software is applied to predict the profiles of the gold nanostructures fabricated in our experiments, and high coincidence is demonstrated between the simulation and the profiles of the fabricated nanostructures examined under

X. Zhou and N. Zhang are with Institute of Materials Research and Engineering, A*STAR (Agency for Science, Technology and Research), 3 Research Link, Singapore 117602 (donna-zhou@imre.a-star.edu.sg, n-zhang@imre.a-star.edu.sg).

World Academy of Science, Engineering and Technology
International Journal of Materials and Metallurgical Engineering
Vol:4, No:8, 2010

scanning electron microscope (SEM) and atomic force microscope (AFM).

## II. PROFILE SIMULATION OF NANOSTRUCTURES OBTAINED BY DISPERSED NSL

As dispersed NSL produces metal nanostructures with numerous varieties in shape, it is important to conduct the profile simulation for the nanostructures based on the factors including nanosphere size, metal evaporation angle and thickness, conformal or non-conformal metal deposition, etc. Our simulation method can be used to predict and design the profile of metal nanostructures for LSPR application.

### A. Nanostructure profile after oblique metal evaporation

To fabricate the metal nanostructures by dispersed NSL, the nanospheres dispersed on a substrate are evaporated with a layer of metal film [17], [18]. As shown in Fig. 1(a), according to the nanosphere diameter $r$, the metal evaporation thickness $t$ and the evaporation angle $\theta$, the metal on the substrate can either be detached from the metal on the nanosphere under the condition of $r\sin\theta + t\cos\theta < r$ to form a 2D nanostructure on the substrate; or be attached to the metal on the nanosphere to form a 3D nanostructure, and the 3D nanostructure can either be conformal or non-conformal as illustrated in Fig. 1 (b) and 1(c), respectively.
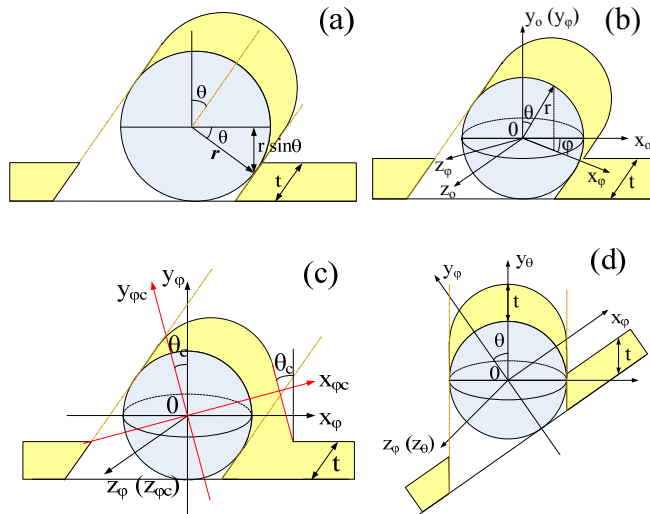


Fig. 1 Metal nanostructure around a nanosphere after oblique metal evaporation. (a) is the condition for the formation of a 2D or 3D nanostructure, (b) is 3D conformal metal nanostructure; (c) is 3D non-conformal metal nanostructure with a non-conformal angle $\theta_c$; (d) is for calculating the thickness of the metal after evaporation in the $x_\theta$-$y_\theta$-$z_\theta$ coordinate system, where the metal looks as if evaporated from the top of the nanosphere.

In order to calculate the profile of the nanostructure after metal evaporation, four inter-transformable coordinate systems are introduced: the original coordinate system $x_o$-$y_o$-$z_o$, where the gold is evaporated at the angles of $\theta$ and $\varphi$ (Fig. 1(b)); the coordinate system $x_\varphi$-$y_\varphi$-$z_\varphi$ (where $y_\varphi = y_o$) with $\varphi = 0$, $\theta \neq 0$ (Fig. 1(b)); the coordinate system $x_\theta$-$y_\theta$-$z_\theta$ (where $z_\theta = z_\varphi$) with $\varphi = 0$, $\theta = 0$ (Fig. 1(d)); and the coordinate system $x_{\varphi c}$-$y_{\varphi c}$-$z_{\varphi c}$ for non-conformal gold deposition (Fig. 1(c)),

where the non-conformal angle $\theta_c$ is the angle between $y_\theta$ and $y_{\varphi c}$.

According to Fig. 1(d), the metal evaporated on the nanosphere has a shape of [18]

$$x_\theta^2 + y_\theta^2 \bigg/ \left(1 + \frac{t}{r}\right)^2 + z_\theta^2 = r^2 \qquad (1)$$

where $t$ is the thickness of the metal, $r$ is the radius of the nanosphere.

When the metal is deposited at a direction with $\theta \neq 0$ and $\varphi = 0$ in the $x_\varphi$-$y_\varphi$-$z_\varphi$ (where $y_\varphi = y_o$) coordinate system, by making the coordinate transformation

$$\begin{cases} x_\theta = x_\varphi \cos\theta - y_\varphi \sin\theta \\ y_\theta = x_\varphi \sin\theta + y_\varphi \cos\theta \end{cases} \qquad (2)$$

the metal deposited on the nanosphere after one deposition at angle $\theta$ is

$$Ay_o^2 - 2Bx_\varphi y_o + Cx_\varphi^2 + z_\varphi^2 - r^2 = 0 \qquad (3)$$

where $A = 1 - T\cos^2\theta$, $B = T\sin\theta\cos\theta$, $C = 1 - T\sin^2\theta$, and $T = \left(\dfrac{2t_k}{r} + \dfrac{t_k^2}{r^2}\right) \bigg/ \left(1 + \dfrac{t_k}{r}\right)^2$.

If $\varphi \neq 0$, one more coordinate transformation of (3) will yield the metal profile on the nanospheres with $\theta \neq 0$ and $\varphi \neq 0$. Because

$$\begin{cases} z_\varphi = -x_o \sin\varphi + z_o \cos\varphi \\ x_\varphi = x_o \cos\varphi + z_o \sin\varphi \\ y_\varphi = y_o \end{cases} \qquad (4)$$

Equation (3) can further be derived as

$$A_1 y_o^2 - 2B_1 y_o + C_1 = 0 \qquad (5)$$

with $A_1 = 1 - Ta_{11}^2$, $B_1 = Ta_{11}a_{22}$, $C_1 = x_o^2 + z_o^2 - r^2 - Ta_{22}^2$, $a_{11} = \cos\theta$, and $a_{22} = \sin\theta(x_o\cos\varphi + z_o\sin\varphi)$.

The areas fulfill $x_\theta^2 + z_\theta^2 < r^2$ has no metal evaporated on the glass substrate, whereas other areas of the substrate have a metal deposition thickness of $t\cos\theta$.

The above formulas are for conformal metal deposition. To calculate the metal profile for non-conformal evaporation, the coordinate system $x_\varphi$-$y_\varphi$-$z_\varphi$ is transferred into $x_{\varphi c}$-$y_{\varphi c}$-$z_\varphi$ by

$$\begin{cases} x_{\varphi c} = x_\varphi \cos\theta_c + y_\varphi \sin\theta_c \\ y_{\varphi c} = -x_\varphi \sin\theta_c + y_\varphi \cos\theta_c \\ z_{\varphi c} = z_\varphi \\ x_\varphi = x_{\varphi c} \cos\theta_c - y_{\varphi c} \sin\theta_c \\ y_\varphi = x_{\varphi c} \sin\theta_c + y_{\varphi c} \cos\theta_c \\ y_\varphi = y_o \end{cases} \qquad (9)$$

by inserting (9) into (3), it is found that

$$A_0 y_{\varphi c}^2 - 2B_{00} x_{\varphi c} y_{\varphi c} + C_{00} x_{\varphi c}^2 + z_\varphi^2 - r^2 = 0 \qquad (10)$$

where $A_0 = 1 - T\cos^2(\theta + \theta_c)$, $B_{00} = T\sin(2\theta + 2\theta_c)/2$, $C_{00} = 1 - T\sin^2(\theta + \theta_c)$, and $x_{\varphi c}$, $y_{\varphi c}$, and $z_\varphi$ are obtained by inserting (4) to (9) as following

World Academy of Science, Engineering and Technology
International Journal of Materials and Metallurgical Engineering
Vol:4, No:8, 2010

$$\begin{cases} x_{\varphi c} = x_o \cos\varphi\cos\theta_c + y_o \sin\theta_c + z_o \sin\varphi\cos\theta_c \\ y_{\varphi c} = -x_o \cos\varphi\sin\theta_c + y_o \cos\theta_c - z_o \sin\varphi\sin\theta_c \\ z_{\varphi c} = z_\varphi = -x_o \sin\varphi + z_o \cos\varphi \end{cases} \quad (11)$$

According to the gold profile on the nanosphere derived in (10), its tangent surface for the non-conformal structure is the surface that has only one intersection point with the gold profile in the $x_{\varphi c}$-$y_{\varphi c}$-$z_\varphi$ coordinate system, i.e., (10) should only have one solution for $y_{\varphi c}$. So the equation for calculating the non-conformal structure is obtained as

$$B_{00}^2 x_{\varphi c}^2 = A_0(C_{00}x_{\varphi c}^2 + z_\varphi^2 - r^2) \quad (12)$$

which can be simplified and expressed in the $x_{\varphi c}$-$y_{\varphi c}$-$z_{\varphi c}$ coordinate system as

$$(1-T)x_{\varphi c}^2 + A_0 z_{\varphi c}^2 - A_0 r^2 = 0 \quad (13)$$

where $A_0 = 1 - T\cos^2(\theta + \theta_c)$, $T = \left(\dfrac{2t_k}{r} + \dfrac{t_k^2}{r^2}\right)\Big/\left(1 + \dfrac{t_k}{r}\right)^2$, $\theta$ is the gold evaporation angle, $\theta_c$ is the non-conformal angle in Fig. 1(c).

### B. Non-conformal metal evaporation at a vertical angle

Based on our experimental observations under AFM, when gold was vertically evaporated onto the dispersed nanospheres, there was a slope on the sidewalls of the gold nanoholes after the removal of nanospheres. This means the vertical metal evaporation is non-conformal. Depending on the non-conformal angle $\gamma$, two cases are shown in Fig. 2, where in the case of angle 1, the nanohole sidewall is a part of a cone with slope $\gamma$; whereas in the case of angle 2, a part of the nanohole forms a part of a cone with slope $\gamma$, whereas its other parts fill around the bottom of the nanosphere. In the $x_o$-$y_o$-$z_o$ coordinate system, the slope $\gamma$ can be expressed as

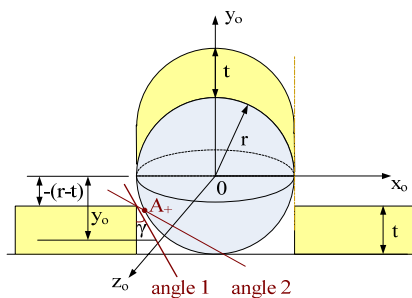$$ctg\gamma = \frac{r - \sqrt{x_o^2 + z_o^2}}{-r + t - y_o} \quad (14)$$



Fig. 2 Non-conformal vertical gold evaporation for calculating the profile of the nanohole with a slant sidewall, which comprises two cases for different non-conformal angle $\gamma$.

For the case of angle 2, point $A_+$ in Fig. 2 can be found by

$$\begin{cases} ctg\gamma(r - \sqrt{x_o^2 + z_o^2}) = -r + t - y_o \\ x_o^2 + z_o^2 + y_o^2 = r^2 \end{cases} \quad (15)$$

Let $F = r - t + r \cdot ctg\gamma$, $A_+$ is solved to be

$$A_+ = F\sin\gamma\cos\gamma \pm \sin\gamma\sqrt{r^2 - F^2\sin^2\gamma} \quad (16)$$

In the case of angle 2, for a specific point $(x_o, z_o)$ on the $x_o$-$z_o$ plane, if $A_+ < \sqrt{x_o^2 + z_o^2} \le r$, the metal thickness at this point is calculated through (14); if $0 < \sqrt{x_o^2 + z_o^2} \le A_+$, the thickness is calculated by the profile of bottom part of the nanosphere.

### III. PROFILE SIMULATION OF NANOSTRUCTURES OBTAINED BY CLOSELY PACKED NSL

Closely packed NSL has the advantages of cost-effectively obtaining periodic metal nanostructures on a substrate. By vertically evaporating metal onto the nanospheres, the metal nanocaps on the nanospheres can be used for LSPR generation [30], [31]. When the nanospheres are removed, nanotriangles are left on the substrate, which have been fabricated by many research groups as classic metal nanostructures for LSPR measurements [4], [5], [26], [32]. The shapes of the nanocaps and the nanotriangles can be trimmed by evaporating the metal at a small oblique angle.

To evaporate metal at a large oblique angle is called glancing angle deposition, where no metal will exist in the flaws of the nanospheres on the substrate and only patchy nanoparticles are generated on the top of the nanospheres due to the shadowing effect of several adjacent nanospheres. It is demonstrated in this paper that the patchy gold nanoparticles on polystyrene nanospheres render sensitive LSPR responses.

However, when the metal is evaporated at an angle between the range of near vertical deposition and glancing angle deposition, depending on the nanospheres' size and arrangement, the metal might be on anywhere of the nanospheres and the substrate with various sizes and shapes, thus the 3D profiles of the nanostructures on the nanospheres and the substrate are simulated.

The formulas for calculating the gold evaporated onto each closely packed nanosphere is the same as in (1)-(5). However, the shadows of its adjacent nanospheres should be considered. When the part of the nanosphere is shadowed by another nanosphere, there will be no gold on this part.

A monolayer of nanospheres closely packed in hexagon is as shown in Fig. 3(a). As long as enough adjacent nanospheres are considered for the shadowing effect, the angle $\varphi$ that needs to be considered is in the range of 0 to 30°, other angles of $\varphi$ will repeat theses profiles.
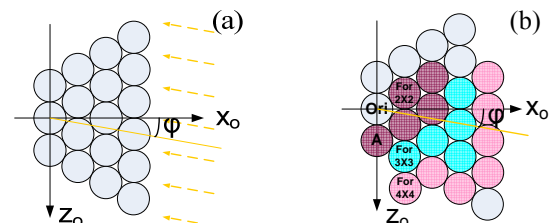


Fig. 3 Profile calculation for hexagonally packed nanospheres in monolayer. (a). shows the azimuthal angle $\varphi$ needs to be considered is in the range of 0 to 30°, (b) shows the adjacent nanospheres need to be considered for calculating a specific nanosphere "Ori". Besides the nanosphere "A", either adjacent 2 × 2 (in purple), 3 × 3 (in amber plus the ones in purple), or 4 × 4 (in pink plus the ones in purple and in amber) arrays of nanospheres should be considered.

World Academy of Science, Engineering and Technology
International Journal of Materials and Metallurgical Engineering
Vol:4, No:8, 2010

Enough number of adjacent nanospheres should be considered to attain an authentic profile of the metal nanostructures on a nanosphere. As presented in Fig. 3(b), to calculate the metal nanostructure on a particular nanosphere specified as "Ori", for hexagonally packed nanospheres in monolayer, at least 5 nanospheres around it should be counted: besides the one beneath the "Ori" which is denoted as "A", the other 4 in purple form a 2 × 2 matrix for shadow calculations. Or in addition to the nanosphere "A", the other 9 nanospheres around it are calculated, which form a matrix of 3 × 3. Similarly, a 4 × 4 or 5 × 5 matrix can be calculated and so on. The more adjacent nanospheres are calculated for the shadowing effect, the more accurate the profile of the nanostructure is.

## IV. EXPERIMENTS

This section demonstrates our LSPR experiments conducted with some nanostructures uniquely fabricated in our group. The LSPR spectrum, optical polarity, and detection sensitivity depend on the profile of these nanostructures, which is determined by the fabrication process in NSL and can be controlled by our simulations.
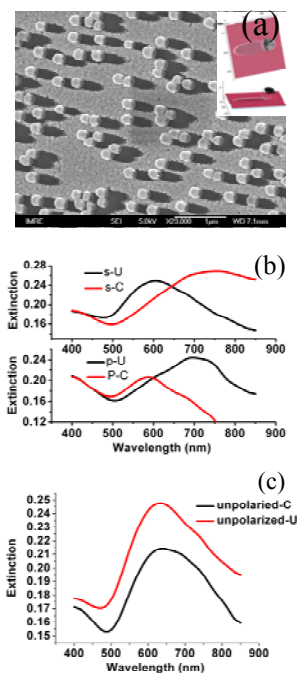
### A. 3D gold nanostructures on nanospheres



Fig. 4 (a). Fabricated and simulated gold 3D nanostructures, and their UV-vis extinction spectra with (b) polarized light and (c) unpolarized light. U means the shadows of gold nanostructures are vertical, C means the shadows are horizontal; p is with vertical electrical field, and s is with horizontal electrical field.

3D metal nanostructures formed by oblique metal evaporation in dispersed NSL can be directly used for LSPR detection. The 3D nanostructures shown in Fig. 4(a) were fabricated by evaporating 30 nm of gold at 70° onto 170 nm

diameter polystyrene nanospheres dispersed on a glass substrate. The insets in Fig. 4(a) are simulated top view and side view of the 3D nanostructures, which demonstrate a good coincidence with the SEM image taken from the top of the nanostructures.

Such a kind of gold nanostructures is polarization dependent. In Fig. 4(b), s-U and p-C have the same LSPR light extinction peak around 590 nm, because the polarization of the light is perpendicular to the gold deposition direction; whereas s-C and p-U have the same LSPR peak around 730 nm, because the polarization of the light is parallel to the gold deposition direction. It should be noted that the slight difference between s-U and p-C, as well as s-C and p-U is a result of ex-situ LSPR measurements. The LSPR spectra will be somewhat different because the gold evaporation angle is different at various locations of the sample, results in different profiles of the gold nanostructures. LSPR is so sensitive that in-situ test will greatly improve the LSPR sensor's sensitivity and accuracy. Fig. 4(c) demonstrates that the LSPR spectrum with unpolarized light shows the same spectrum for C- and U-shaped nanostructures, since it is the superposition of the two spectra of s-C and p-C, or the superposition of s-U and p-U. The unpolarized light can be used for LSPR sensing, but polarized light can tune the extinction peak of LSPR up to hundreds of nanometers, which is difficult to achieve by changing the shape of the gold nanostructures, thus this can be regarded as an advantage of the polarization dependent gold nanostructures for LSPR.
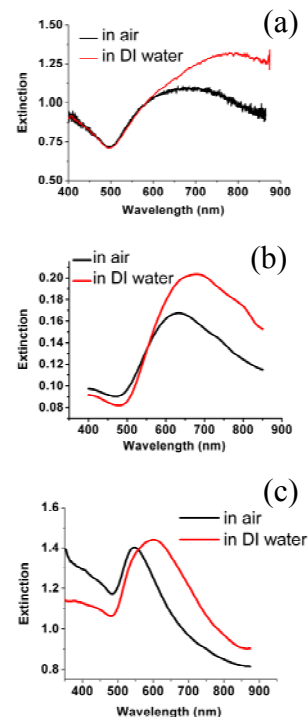


Fig. 5 LSPR spectra when the adjacent media are air and deionized (DI) water for various gold nanostructures. (a) 50 nm of gold was evaporated onto the 170 nm diameter polystyrene nanospheres at 70°; (b) 30 nm of gold was evaporated at 70° onto the same kind of nanospheres; (c) when the nanospheres in (b) were burnt. The LSPR

World Academy of Science, Engineering and Technology
International Journal of Materials and Metallurgical Engineering
Vol:4, No:8, 2010

sensitivities for (a)-(c) are respectively 317, 242, and 170 nm/RIU, RIU is the refractive index unit.

It is also find that the LSPR sensitivity is very sensitive to the gold thickness and the existence of the polystyrene nanospheres. Fig. 5(a) shows the spectra when 50 nm of gold was evaporated onto 170 nm diameter nanospheres at 70˚. The extinction peak of the LSPR spectrum shifts 104 nm when the medium is changed from air to water, and thus gives a sensitivity of 317 nm/RIU, RIU is the refractive index unit. Fig. 5(b) presents when 30 nm of gold is evaporated at 70˚ (as shown in Fig. 4(a)), the LSPR spectra yield a LSPR sensing sensitivity of 242 nm/RIU, and the spectral bandwidth is narrower. Fig. 5(c) presents the LSPR spectra of the same gold nanostructures of Fig. 5(b), when the polystyrene nanospheres were burnt up at a high temperature in an oven. In this case, the bandwidth of the LSPR spectra is further reduced, but it renders a sensitivity of only 170 nm/RIU.

It seems that when the gold thickness is reduced or the polystyrene nanospheres are removed, the LSPR spectra can be sharpened. But the decrease in the bandwidth of the LSPR spectra blue shifted the LSPR peaks and thus reduced the sensitivity of the LSPR sensing. Even so, in the optimization of our gold nanostructure fabrications, narrower LSPR spectrum is preferred, because this gives clearer identification of small LSPR spectrum shift and overall it is expected to provide a higher signal to noise ratio in LSPR detections.

### B. Nanoholes with slant sidewalls

Nanoholes were fabricated by dispersing 110 nm-diameter polystyrene nanospheres on a 2 cm × 2 cm glass substrate [19], evaporating 40 nm of gold film onto the nanospheres, and removing the nanospheres by sonication in water for 40 seconds.
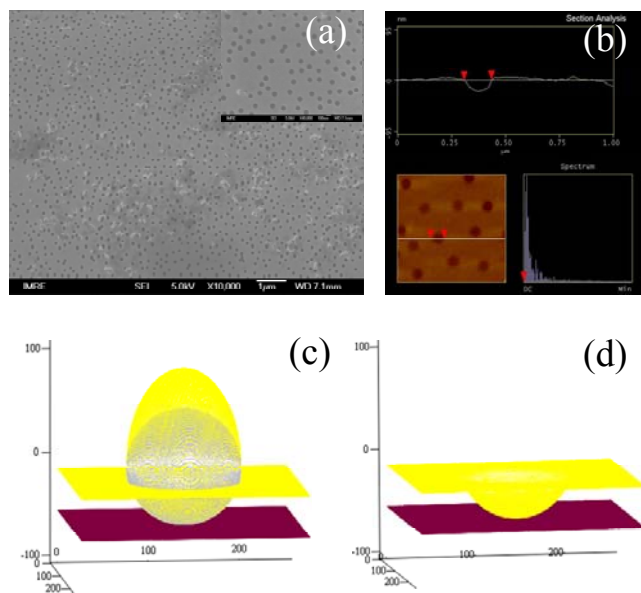


Fig. 6 SEM and AFM images of 40 nm thick gold nanoholes with 110 nm diameter. (a) is the SEM image, (b) shows the AFM image and the cross section of the nanoholes, (c) is the simulated profile after 40 nm gold evaporation at a non-conformal angle of 45˚, (d) is the simulated shape of the nanohole on the substrate after removing the nanospheres.

The SEM images of the fabricated nanoholes are shown in Fig. 6(a), where the density of our nanoholes is about $3/\mu m^2$ and the average interval of the nanoholes is 2 times of the diameter. The AMF image in Fig. 6(b) indicates that the nanohole's cross section is not a square but a slope. This is due to the non-conformal gold evaporation in the thermal evaporator, as the capillary force attracted gold atoms to deposit under the nanospheres during gold evaporation. Such a profile is different from previously reported nanoholes with vertical sidewalls [14], [15], [33], and it benefits the bonding of more biomolecules in the plasmonic enhanced area.

The simulated gold profile after gold evaporation is presented in Fig. 6(c), and the nanohole obtained after the removal of the nanosphere is shown in Fig. 6(d). In these simulations, it is supposed that the non-conformal angle γ is 45˚. It can be observed that Fig. 6(d) has the same profile as the one measured by AFM in Fig. 6(b).

By measuring the nanohole sample in air and water, and taking a glass substrate with a gold thin film evaporated at the same thickness of the nanoholes as a reference [19], the sample indicates a LSPR sensitivity of 36 nm/RIU. The lower sensitivity compared to 100 nm/RIU for 110 nm-dia nanoholes in [14] is due to the lower aspect ratio of our nanoholes, as the gold is thicker in our samples. However, due to the slant sidewalls of the nanoholes in our sample, the biotin-streptavidin immunoassay measurement of this sample demonstrates satisfactory sensitivity for biological tests [19].
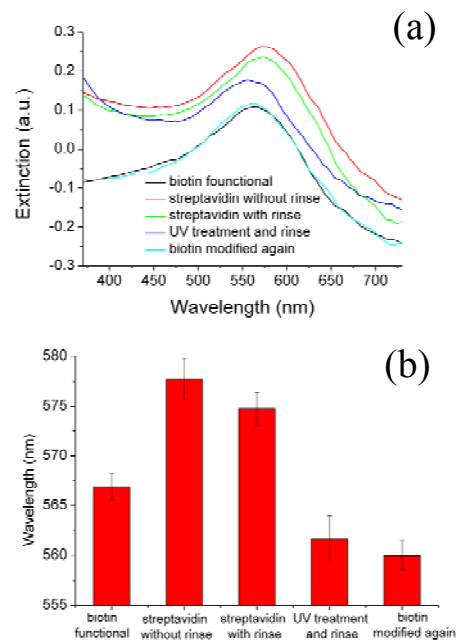


Fig. 7 Biotin-streptavidin immunoassay measured by the nanoholes. (a) shows the extinction spectra, (b) shows the error bars for the LSPR peaks at different locations of the sample, as the nanoholes are quite uniform on the whole 2 cm × 2 cm sample.

The biotin-streptavidin immunoassay was studied with a nanohole sample in several steps, and the LSPR spectrum was taken after each step. Firstly, the sample was immersed into biotinylated thiol at the concentration of 374 µM in ethanol for

World Academy of Science, Engineering and Technology
International Journal of Materials and Metallurgical Engineering
Vol:4, No:8, 2010

20 hours at room temperature to form a self assembled monolayer of biotin, then the sample was rinsed with ethanol and deionized (DI) water and nitrogen dried. Secondly, the sample was immersed into 1 µM streptavidin in PBS for 20 hours at room temperature, dried without rinse. Thirdly, the sample was rinsed repeatedly with ethanol, PBS and DI water and nitrogen dried. Fourthly, the sample was exposed under a UV cleaner for 30 minutes to break the chemical bond between the thiol and gold, then the sample was rinsed with ethanol, PBS and DI water repeatedly and nitrogen dried. Fifthly, the sample was incubated with biotinylated thiol in ethanol for 20 hours at room temperature again, rinsed and dried.

For the biotin-streptavidin immunoassay, its LSPR extinction spectra are plotted in Fig. 7. The nanohole sample modified with biotin had a LSPR peak at 567 nm. After incubation in streptavidin and dried, the LSPR peak red-shifted to 578 nm and exhibited a prominent 11 nm shift, due to the local dielectric change induced by streptavidin bonding. Repeated rinse of ethanol, PBS and DI water only blue-shifted the wavelength 3 nm, because some unspecific bonded substances on the sample were washed away. Biotin and streptavidin were chemically bonded on gold, and the LSPR peak shift was mainly contributed from the streptavidin at the circumferences of the nanoholes. As the density of our nanoholes was about $3/\mu m^2$, the area for detection is 5 mm in diameter defined by the spot size of the illumination light, based on the size/shape of the nanohole and streptavidin (SA) [4], there were about 218 SA around each nanohole, therefore, the effective number of streptavidin under detection for a sample was estimated to be $1.28 \times 10^{10}$, i.e., 21.3 fMol/sample. This is about 3 times of the limit of detection (LOD) reachable by silver nanotriangles measured in nitrogen gas environment, where $4.6 \times 10^9$ SA/sample, equivalent to 7.6 fMol/sample, was reported by Northwestern University [4]. However, silver has higher LSPR sensitivity, and it will be oxidized in air.

After UV exposure and rinse, the LSPR peak turned to 561.7 nm, as the UV exposure broke the bond between biotinylated thiol and gold. No obvious extinction intensity change at this step was observed, which inferred the biotin and streptavidin were not washed away. After incubating the UV exposed sample with biotinylated thiol in ethanol, the intensity of the sample's LSPR extinction peak returned to its original, because the streptavidin nearby the nanoholes were dragged away by excessive biotin in ethanol. This means the sample is reusable, thus the cost of the device can be further reduced.

### C. Patchy gold nanoparticles on nanospheres

Although silver nanotriangles fabricated by closely packed NSL has been intensively investigated, here it is demonstrated for the first time that patchy gold nanoparticles on the top of polystyrene nanospheres can be utilized for LSPR detections with high sensitivity.

In closely packed NSL, defects tend to happen at a critical length longer than 10 – 100 µm. The defects change the orientation, i.e., the azimuthal angle φ, of the nanospheres and thus vary the shape of the nanostructures. According to the study of Kretzschmar's group [27], at small deposition angle θ, the shape of the patch on the nanospheres are not so sensitive to the azimuthal angle φ, whereas only at large deposition angle, the shape of the patchy varies dramatically at different φ. In our experiment, patchy gold nanoparticles were obtained at 85° for LSPR measurement, and the challenge was to reduce the defects in the closely packed NSL.

The 500 nm-diameter polystyrene nanospheres were dropped onto a clean glass substrate to self-assemble into a hexagonally close packed monolayer. The samples were deposited with 50 nm of gold in a thermal evaporator at θ = 85°, and the patchy gold nanoparticles were formed on the top of the nanospheres, as photographed in Fig. 8(a). The inset in Fig. 8(a) shows that the simulation is consistent with the SEM image.
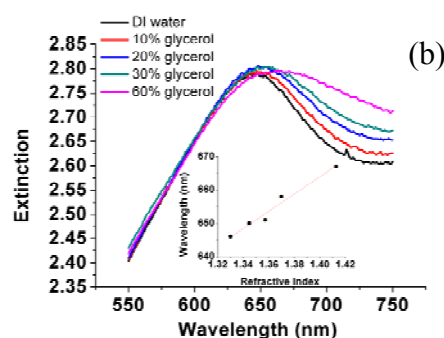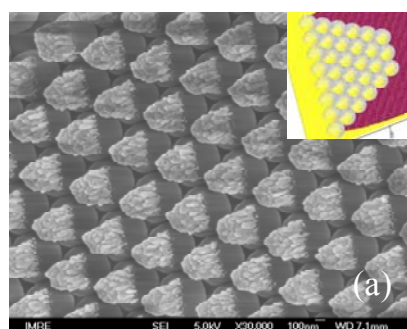


Fig. 8 (a) is the SEM image of the nanospheres with patchy gold nanoparticles fabricated, by evaporating 50 nm of gold at 85° onto 500 nm diameter polystyrene nanospheres, inset shows the simulated shape. (b) LSPR measurements of the patchy nanoparticles with media of different refractive indices. The inset shows the wavelength shift of the LSPR peak versus the refractive index increase.

To examine the LSPR sensitivity of the patchy nanoparticles, the refractive index of the nanoparticles' adjacent medium was adjusted by using glycerol solutions at different concentrations. In the experiments, the solution and the LSPR chip were confined in a transparent fluidic chamber, the chip's transmission spectra were taken as shown in Fig. 8(b). The LSPR extinction peak red-shifted linearly with the refractive index variation, varied from 645 to 670 nm, and rendered a LSPR sensitivity of 258 nm/RIU.

### V. CONCLUSION

This paper described three gold nanostructures developed in our group with nanosphere lithography for LSPR detections. For dispersed NSL, 3D gold nanostructures on polystyrene

World Academy of Science, Engineering and Technology
International Journal of Materials and Metallurgical Engineering
Vol:4, No:8, 2010

nanospheres, gold nanoholes with slant sidewalls were proposed; and for closely packed NSL, patchy gold nanoparticles on polystyrene nanospheres were investigated. Since the nanostructures fabricated by NSL have an abundance of different shapes, and each shape renders a different LSPR spectrum and LSPR sensitivity, 3D profile simulation for these nanostructures were conducted to control the shape of desired metal nanostructures for LSPR, and good correlations between the fabrication and simulation were verified. Our LSPR measurements demonstrated that these cost-effective nanostructures have satisfactory sensitivities on the detections of biotin-streptavidin immunoassay, or glycerol solutions at different concentrations.

REFERENCES

[1] C. F. Bohren and D. R. Huffman, "Absorption and Scattering by Small Particles", New York: Wiley Interscience, 1983.
[2] E. Hutter and J. H. Fendler, "Exploitation of localized surface plasmon resonance," *Adv. Mater.,* vol. 16, 1685–1706, 2004
[3] B. Sepulveda, P. C. Angelome, L. M. Lechuga, and L. M. Liz-Marzan, "LSPR-based Nanobiosensor," *Nano Today*, vol. 4, pp. 244–251, 2009.
[4] A. J. Haes and R. P. Van Duyne, "A nanoscale optical biosensor: Sensitivity and selectivity of an approach based on the localized surface plasmon resonance spectroscopy of triangular silver nanoparticles," *J. Am. Chem. Soc.*, vol. 124, pp. 10596–10604, 2002.
[5] J. C. Riboh, A. J. Haes, A. D. McFarland, C. R. Yonzon, and R. P. Van Duyne, "A nanoscale optical biosensor: real-time immunoassay in physiological buffer enabled by improved nanoparticles adhesion," *J. Phys. Chem. B*, vol. 107, pp. 1772–1780, 2003.
[6] J. N. Anker, W. P. Hall, O. Lyandres, N. C. Shah, J. Zhao and R. P. Van Duyne, "Biosensing with plasmonic nanosensors," *Nat. Mater.*, vol. 7, pp. 442–453, June 2008.
[7] M. E. Stewart, C. R. Anderton, L. B. Thompson, J. Maria, S. K. Gray, J. A. Rogers, and R. G. Nuzzo, "Nanostructured plasmonic sensors," *Chem Rev.*, vol. 108, pp. 494–521, February 2008.
[8] M. Fleischmann, P. J. Hendra, and A. J. Mcquillan, "Raman spectra of pyridine adsorbed at a silver electrode," *Chem. Phys. Lett.*, vol. 26, pp. 163–166, 1974.
[9] K. Kneipp, H. Kneipp, I. Itzkan, R. Dasari, and M. Feld, "Ultrasensitive chemical analysis by Raman spectroscopy," *Chem. Rev.*, vol. 99, pp 2957–2975, 1999.
[10] I. H. El-Sayed, X. Huang, and M. A. El-Sayed, "Selective laser photo-thermal therapy of epithelial carcinoma using anti-EGFR antibody conjugated gold nanoparticles," *Cancer Lett.*, vol. 239, pp. 129–135, 2006.
[11] T. A. Larson, J. Bankson, J. Aaron, and K. Sokolov, "Hybrid plasmonic magnetic nanoparticles as molecular specific agents for MRI/optical imaging and photothermal therapy of cancer cells," *Nanotechnology*, vol. 18, pp. 1–8, 2007.
[12] J. S. Shumaker-Parry, H. Rochholz, and M. Kreiter, "Fabrication of crescent-shaped optical antennas," *Adv. Mater.*, vol. 17, pp. 2131–2134, 2005.
[13] H. Rochholz, N. Bocchio, and M. Kreiter, "Tuning resonances on crescent-shaped noble-metal nanoparticles," *New J. Phys.*, vol. 9, 53, 2007.
[14] J. Prikulis, P. Hanarp, L. Olofsson, D. Sutherland, and M. Käll, "Optical spectroscopy of nanometric holes in thin gold films," *Nano Lett.*, vol. 4, pp. 1003–1007, 2004.
[15] D. Gao, W. Chen, A. Mulchandani, and J. S. Schultz, "Detection of tumor markers based on extinction spectra of visible light passing through gold nanoholes," *Appl. Phys. Lett.*, vol. 90, 073901, 2007.
[16] Y. Lu, G. L. Liu, J. Kim, Y. X. Mejia, and L. P. Lee, "Nanophotonic crescent moon structures with sharp edge for ultrasensitive biomolecular detection by local electromagnetic field enhancement effect," *Nano Lett.*, vol. 5, pp. 119–124, 2005.
[17] X. Zhou, S. Virasawmy, W. Knoll, K. Y. Liu, M. S. Tse, and L. W. Yen, "Profile simulation and fabrication of gold nanostructures by separated nanospheres with oblique deposition and perpendicular etching," *Plasmonics*, vol. 2, pp. 217–230, 2007.

[18] X. Zhou, W. Knoll, K. Y. Liu, M. S. Tse, S. Oh, and N Zhang, "Design and fabrication of gold nanostructures with dispersed nanospheres for localized surface plasmon resonance applications," *J. Nanophotonics*, vol. 2, 023502, 2008.
[19] G. Xiang, N. Zhang, and X. Zhou, "Localized surface plasmon resonance biosensing with large area of gold nanoholes fabricated by nanosphere lithography," *Nanoscale Res. Lett.*, vol. 5, pp. 818–822, 2010.
[20] X. Zhou, N. Zhang, and C. Tan, "Profile prediction and fabrication of wet etched gold nanostructures for localized surface plasmon resonance," *Nanoscale Res. Lett.*, vol. 5, pp. 344–352, 2010.
[21] S. M. Yang, S. G. Jang, D. G. Choi, S. Kim, and H. K. Yu, "Nanomachining by colloidal lithography," *Small*, vol. 2, pp. 458–475, 2006.
[22] B. J. Y. Tan, C. H. Sow, T. S. Koh, K. C. Chin, A. T. S. Wee, and C. K. Ong, "Fabrication of size-tunable gold nanoparticles array with nanosphere lithography, reactive ion etching, and thermal annealing," *J. Phys. Chem. B*, vol. 109, pp. 11100–11109, 2005.
[23] G. Zhang, D. Wang, and H. Möhwald, "Patterning microsphere surfaces by templating colloidal crystals," *Nano Lett.*, vol. 5, pp. 143–146, 2005.
[24] G. Zhang, D. Wang, and H. Möhwald, "Nanoembossment of Au patterns on microspheres," *Chem. Mater.*, vol. 18, pp. 3985–3992, 2006.
[25] G. Zhang, D. Wang, and H. Möhwald, "Ordered binary arrays of Au nanoparticles derived from colloidal lithography," *Nano Lett.*, vol. 7, pp. 127–132, 2007.
[26] T. Jensen, M. Malinsky, C. Haynes, and R. Van Duyne, "Nanosphere lithography: tunable localized surface plasmon resonance spectra of silver nanoparticles," *J. Phys. Chem. B*, vol. 104, pp. 10549–10556, 2000.
[27] A. B. Pawar and I. Kretzschma, "Patchy particles by glancing angle deposition," *Langmuir*, vol. 24, pp.355–358, 2008.
[28] A. B. Pawar and I. Kretzschmar, "Multifunctional patchy particles by glancing angle deposition," *Langmuir,* vol. 25, pp. 9057–9063, 2009.
[29] X. Zhou, K. Y. Liu, W. Knoll, C. Quan, and N. Zhang, "3D profile simulation of metal nanostructures obtained by closely-packed nanosphere lithography," *Plasmonics*, vol. 5, pp. 141–148, 2010.
[30] T. Endo, K. Kerman, N. Nagatani, H. M. Hiepa, D-K. Kim, Y. Yonezawa, K. Nakano, and E. Tamiya, "Multiple label-free detection of antigen-antibody reaction using localized surface plasmon resonance-based core-shell structured nanoparticle layer nanochip," *Anal. Chem.*, vol. 78, pp. 6465–6475, 2006.
[31] T. Endo, K. Kerman, N. Nagatani, Y. Takamura, and E. Tamiya, "Label-free detection of peptide nucleic acid-DNA hybridization using localized surface plasmon resonance based optical biosensor," *Anal Chem.*, vol. 77, pp. 6976–6984, November 2005.
[32] C. R. Yonzon, E. Jeoung, Zou S, G. C. Schatz, M. Mrksich, and R. P. Van Duyne, "A comparative analysis of localized and propagating surface plasmon resonance sensors: The binding of Concanavalin A to a monosaccharide functionalized self-assembled monolayer," *J. Am. Chem. Soc.*, vol. 126, pp. 12669–12676, 2004.
[33] T. Rindzevicius, Y. Alaverdyan, A. Dahlin, F. Höök, D. S. Sutherland, and M. Käll, "Plasmonic sensing characteristics of single nanometric holes," *Nano Lett.*, vol. 5, pp. 2335–2339, 2005.

**X. Zhou** is a Research Scientist in the Institute of Materials Research and Engineering (IMRE), A*STAR (Agency for Science, Technology and Research), Singapore. She received her BE, ME and PhD degrees in electro-photonics from Zhejiang University, China in 1989, 1992 and 1995, respectively. Her current research is optical related MEMS fabrication, nanostructure fabrication for LSPR bio-sensors, and optical simulations.
**N. Zhang** is a Research Engineer in the Institute of Materials Research and Engineering (IMRE), A*STAR (Agency for Science, Technology and Research), Singapore. She received her BE in polymer chemical engineering from Beijing University of Chemical Technology in 1999 and her MS in materials science from National University of Singapore in 2005. Her current research interests include optical detection and biosensors based on surface plasmon resonance and localized surface plasmon resonance.